Research Article

Influence of holmium ions on the structural and optical properties of barium tellurite glasses

P. Vani [a], G. Vinitha [a], R. Praveena [b], M. Durairaj [c], T.C. Sabari Girisun [c], N. Manikandan [a],[*]

[a] *Division of Physics, School of Advanced Sciences, Vellore Institute of Technology, Chennai, 600127, India*
[b] *Department of Physics, Gayatri Vidya Parishad College of Engineering, Visakhapatnam, 530048, India*
[c] *School of Physics, Bharathidasan University, Tiruchirappalli, 620 024, Tamil Nadu, India*

ABSTRACT

Barium tellurite glasses doped with holmium ions [$60TeO_2 + 20ZnO + 4BaF_2 + (16-x) BaCO_3 + xHo_2O_3$ ($0.25 \geq x \leq 2$)] synthesized using melt quenching technique have been explored for their optical applications. Compositional tuning led to a maxima and minima in their respective optical bandgap (4.079 eV) and refractive index (2.154) values around 0.75 mol%. Green emission corresponding to the $^5I_8 \rightarrow \, ^5F_4$ ($^5S_2$) transition was found to be dominant in the visible region, with a reduction in intensity beyond 0.75 mol.%. This indicated the occurrence of concentration quenching effects and the limit of doping for obtaining high emission intensities. On exposure to nanosecond pulses of 532 nm wavelength, all samples showed good optical non-linearity when investigated using Z-scan technique. Open aperture scans showed reverse saturable absorption behavior owing to two photon absorption process. With reduced limiting threshold values, all compositions in this glass tie-line were found to act as good optical limiters, leading to the possibility of forming efficient limiting devices.

1. Introduction

Rare earth (RE^{3+}) doped materials with their excellent luminescence properties have profound applications in the domains of optoelectronics like lasers, light sources, sensors etc. These ions are found to exhibit efficient energy level splitting and energy level broadening owing to 4f-4f electronic interactions [1]. The luminescence wavelengths vary from ultraviolet to mid-infrared depending on the type of ion. There are various ions which yield multiple wavelength transitions, which depend on the host material. Compared to crystal host, glasses possess higher RE^{3+} ion solubility, higher transparency, wide compositional variance etc., which makes them suitable host for achieving various devices exploiting their optical properties [2]. Different glasses like germanates, silicates, fluoro-germanates, fluoroborates, fluorophosphates etc., have been utilized as host glasses for RE^{3+} ion incorporation and have been explored for their optical applications [3–7]. Among various glass matrices, tellurite glasses form an excellent host matrix for these ions owing to their inherent properties like lower phonon energy, lesser glass transition temperature, higher refractive index etc. Lower phonon energy helps in reducing the non-radiative transitions and improving radiative transitions leading to improved lasing ability [8–10].

Among RE^{3+} ions, holmium finds applications in different domains owing to their broader energy level distribution across different wavelength regions in visible as well as infrared. Their efficient lasing ability has been related to their low-lying metastable levels [11–13]. Green emission was found to be dominant among other visible emissions in hosts like titano lead borate and lead silicate glasses [14,15]. Similar visible light emissions have been reported in different host glasses [16, 17]. Most of the reports have also shown a decrease in emission intensity beyond 1 mol% of holmium ions, indicating the effect of concentration in altering the optical properties [18]. Considering the nature of these ions and possible applications, it is also necessary to look at other properties beyond optical emission and understand the associated changes that these ions bring to the glass network.

Lasers being one of the dominant applications of these ion doped systems, it becomes necessary to find ways to use them without affecting the material on which the lasing emission is incident. Optical limiters are one such family of materials, which utilize the non-linear optical properties of materials to exhibit such phenomenon. This involves two-photon absorption process, and the output intensity of beam will be limited to a certain maximum value depending on the absorption coefficient of the material. Though various types of samples have been found to possess this capability, recent results have shown that tellurite glasses can act as limiting materials owing to their good optical non-linearity

---

* Corresponding author.
  E-mail address: manikandan.narendran@vit.ac.in (N. Manikandan).

[19–21]. It becomes necessary to check whether doping with RE^{3+} ions which aids emission hinders or facilitates the non-linearity of the base glass. Recent investigations have shown that ions like erbium, thulium etc., aid in limiting ability of these tellurite host glass [22–24], which provides an avenue to look at the behaviour of holmium ions in these glasses.

This work focuses on understanding the effect of doping holmium ions in barium tellurite glasses. Holmium concentration has been limited to 2 mol% and their effect on altering the structural, thermal, linear and non-linear optical properties of these glasses have been explored. Probable device applications as limiting materials and lasing glasses with improved efficiency are also analysed.

2. Experimental

Conventional melt-quenching technique was adopted to synthesize holmium doped barium tellurite glasses with molar compositions, $60TeO_2 + 20ZnO + 4BaF_2 + (16-x) BaCO_3 + xHo_2O_3$ ($0.25 \geq x \leq 2$). Precisely weighed chemicals were mixed, ground and placed in a platinum crucible for melting at 850 °C for 120 min. Then the melted mixture was poured onto a preheated metal plate and annealed for 720 min before it was slowly cooled to room temperature. The glass samples were ground to a fine powder for further spectroscopic examinations. Various compositions with holmium oxide variation from 0.25% to 2.0% is labelled as indicated below.

1. $60TeO_2 + 20ZnO + 4BaF_2 + 15.75BaCO_3 + 0.25Ho_2O_3$ - **TZBBHo$_{0.25}$**
2. $60TeO_2 + 20ZnO + 4BaF_2 + 15.5BaCO_3 + 0.5Ho_2O_3$ - **TZBBHo$_{0.5}$**
3. $60TeO_2 + 20ZnO + 4BaF_2 + 15.25BaCO_3 + 0.75Ho_2O_3$ - **TZBBHo$_{0.75}$**
4. $60TeO_2 + 20ZnO + 4BaF_2 + 15BaCO_3 + 1.0Ho_2O_3$ - **TZBBHo$_{1.0}$**
5. $60TeO_2 + 20ZnO + 4BaF_2 + 14.5BaCO_3 + 1.5Ho_2O_3$ - **TZBBHo$_{1.5}$**
6. $60TeO_2 + 20ZnO + 4BaF_2 + 14BaCO_3 + 2.0Ho_2O_3$ - **TZBBHo$_{2.0}$**

To confirm the amorphous nature of the above-mentioned glasses, X-ray diffraction spectra were recorded using Rigaku X-ray diffractometer (Cu-Kα, λ = 1.54 Å). Various physical properties like glass density, oxygen packing density (OPD), molar volume (V_m), refractive index, molar refractivity etc., were measured and calculated. For density measurement, Archimedes principle with water as an immersion liquid was employed. The error was found to be approximately ±1%. Raman spectra were obtained in the wavenumber range 200–1000 cm^{-1} for the laser excitation wavelength of 532 nm using single grating high resolution aT64000 Horiba-Jobin Yvon spectrometer coupled to liquid nitrogen cooled CCD. The characteristic glass temperatures i.e., onset glass transition temperature, onset crystallization peak and melting temperatures were obtained from measurements using differential scanning calorimetry (DSC, NETZSCH STA 449/C) operated at a constant heating rate of 10 °C/min. Absorption spectra were recorded from UV to NIR region (i.e., 300–2000 nm) using a PerkinElmer Lambda 900 UV–VIS–NIR spectrophotometer with a slit width of 1 nm resolution. Emission spectra were obtained at the excitation wavelength of 362 nm with output recorded between 200 and 800 nm. Decay curves were recorded to obtain the lifetimes of the excited state. Optical limiting threshold values of these glasses were obtained from non-linear absorption data of open aperture Z-scan technique using a Q-switched frequency-doubled Nd: YAG laser (532 nm, 100 μJ, 9 ns). All the measurements were done at room temperature.

3. Results and discussion

3.1. XRD and physical properties

The structural investigation was performed using X-ray diffraction to confirm the amorphous nature of the samples. Fig. 1 exhibits the usual x-
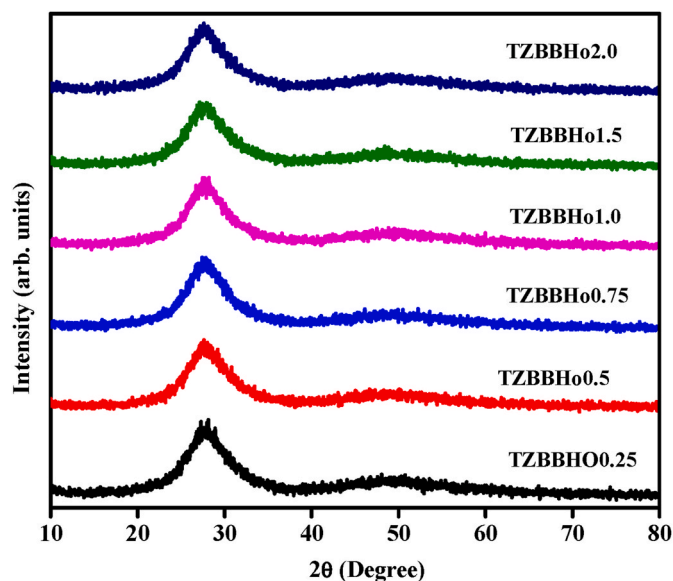

Fig. 1. XRD patterns of the holmium doped barium tellurite glasses.

ray diffraction pattern confirming the amorphous nature with no crystalline peaks. X-ray diffraction patterns were found to be consistent with those of other RE^{3+} doped host glasses [25].

Physical properties like density, molar volume, refractive index etc. were calculated using standard relations and are presented in Table 1 [26–28]. Density of the glass is affected by structural modifications which depends on the coordination number, crosslink density etc., and also allows to analyze various other properties. The increase in density can be attributed to the presence of non-bridging oxygen bonds, leading to open network structure which is also seen from Raman spectra of these samples [29]. Non-monotonic variation in certain other physical properties could be related to the structural changes occurring owing to holmium incorporation, which shows significant changes around 0.75 and 1 mol%. These are normally related to the inter-conversion between bridging and non-bridging oxygen atoms and their increment/decrement owing to dopant incorporation. Measured and calculated results indicate the dominance of the mass of holmium ions in causing a monotonic increase in density as it replaces lighter barium atoms, compared to structural variations owing to bridging and non-bridging sites. Chemical stability of the samples can be elucidated from the lower polarizability values. Metallization values are found to be less than one, indicating their non-metallic nature. Increment in holmium oxide leads to higher non-metallic nature which in general lead to better optical non-linearity [12,30,31].

3.2. Optical and thermal analysis

Optical bandgap is a significant parameter to define the absorption effects of materials. It is useful to examine optically induced electronic transitions, energy gaps and electronic band structure of crystalline and vitreous materials by evaluating the absorption edge in the UV region. The optical band gap is calculated for indirect transition using standard formula [32]. Fig. 2 shows the plot of hν vs. $(\alpha h\nu)^{0.5}$, from which the optical band gap values for $60TeO_2 + 20ZnO + 4BaF_2 + (16-x) BaCO_3 + xHo_2O_3$ glasses (x = 0.25–2.0 mol%) are found out and reported in Table 1. It can be observed that the values increased as the dopant concentration varied from 0.25 mol% to 0.75 mol% and decreased for higher concentrations, indicating the changes in the ratio of non-bridging oxygen atoms (NBO's) to bridging oxygen atoms (BO). The decrease in NBO's lower the valence band minimum causing an increase in the optical band gap values from 0.25 to 0.75 mol% of holmium doped TZBB glass matrices. As the dopant concentrations increases, the

Table 1

Physical properties of Ho^{3+} doped barium tellurite glasses.

| Properties	Sample code					
	TZBBHo0.25	TZBBHo0.5	TZBBHo0.75	TZBBHo1.0	TZBBHo1.5	TZBBHo2.0
Average Molecular weight, M (g/mol)	151.07	151.52	151.97	152.42	153.33	154.23
Density, ρ (g/cm^3) $\pm$ 0.01	5.408	5.41	5.43	5.448	5.473	5.486
Molar Volume, V_m (cm^3/mol)	27.93	28.01	27.99	27.98	28.01	28.11
Oxygen packing density, OPD (g atm/l)	67.22	67.12	67.17	67.19	67.1	66.87
Optical band gap, E_g (eV)	4.032	4.049	4.079	4.02	3.996	3.964
Refractive index, n	2.163	2.160	2.154	2.165	2.170	2.176
Molar refractivity, R_m (cm^3/mol)	15.39	15.40	15.34	15.43	15.49	15.59
Molar Polarizability, α_m ($\times 10^{-24}$ cm^3/mol)	6.10	6.11	6.09	6.12	6.15	6.19
Electronic Polarization, α_e ($\times 10^{-23}$ cm^3)	2.19	2.18	2.18	2.19	2.19	2.20
Metallization Criterion, M	0.448	0.449	0.451	0.448	0.446	0.445
Dielectric Constant, ε	4.678	4.665	4.639	4.687	4.708	4.735
Ho^{3+}ion concentration, N (moles/litre)	0.178	0.357	0.535	0.714	1.070	1.422
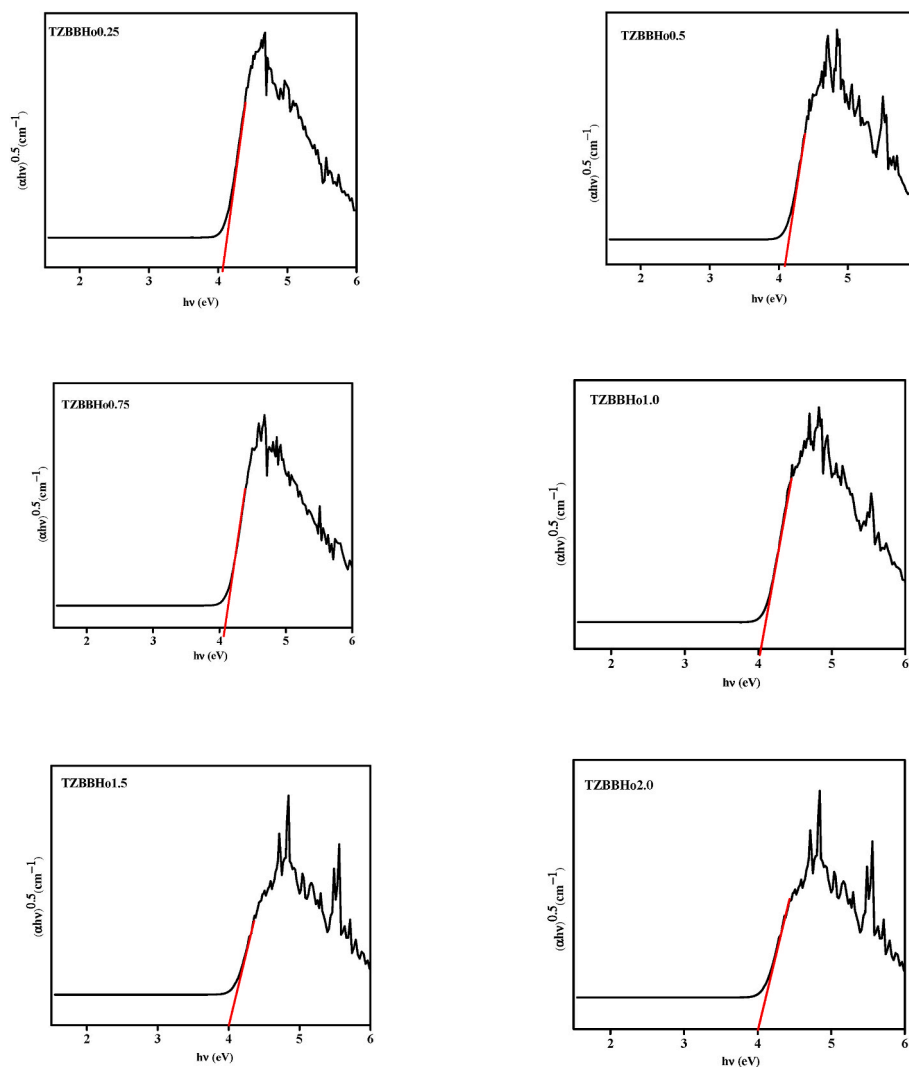
Fig. 2. Tauc plots of Ho^{3+} doped barium tellurite glasses.

ratio of NBO's increases compared to BO leading to a higher value of valence band maximum and hence a consequent decrease in the optical band gap values [18,29,33].

Fig. 3 shows the differential scanning calorimetric curves for all the samples in the temperature range of 30°–600 °C. From the result, the glass transition temperature (T_g), the onset crystallization temperature (T_c), the difference between them $\Delta T = T_c - T_g$, the peak crystallization temperature $\Delta T_p = T_p - T_c$, and the stability parameter $S = (\Delta T * \Delta T_p)/T_g$

were calculated and are listed in Table 2. Thermal stability (ΔT) is a critical characteristic for a wide range of technological applications, one among them being as optical fibers. Since fiber drawing involves reheating process from the glassy state, any crystallization that happens during the process increases scattering loss, affecting the optical transmission properties of drawn fiber. To prevent this issue and to create a broad operating range, ΔT value must be as high as possible ($\geq$100 °C) [34–36]. According to the ΔT values presented in Table 2, all of the
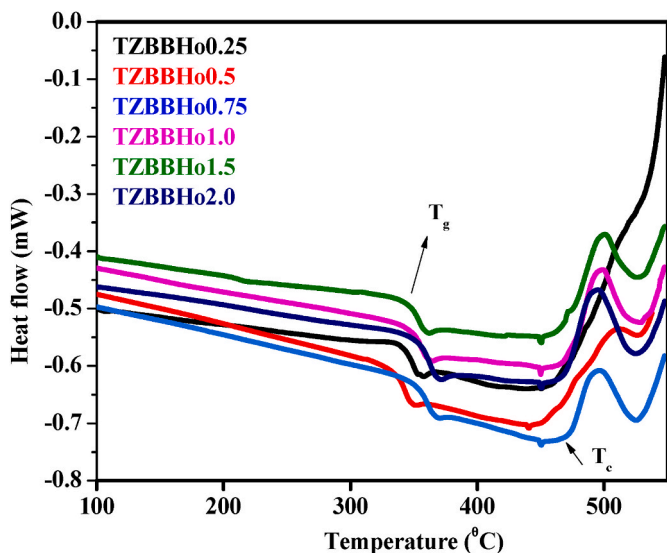
Fig. 3. DSC spectra of Ho^{3+} doped barium tellurite glasses.

samples of Ho^{3+} doped TZBB glasses have high ΔT (≥ 110 °C), which is greater than the typical tellurite glass [37]. As a result, the current glasses possess good thermal stability and durability making them excellent choices for making fiber optic devices.

3.3. Raman spectra

Raman spectroscopy has been employed to analyze the structure and vibrational energies of holmium doped barium tellurite glasses. Raman spectra of these glasses were recorded in the region of 200–1000 cm^{-1} and are shown in Fig. 4a. Spectra show a broad band between 200 and 400 cm^{-1} and 2 significant peaks between 600 and 800 cm^{-1} regions. Dominance of non-bridging bonds in all samples can be identified by the significant intensities of band near 770 cm^{-1}. All the spectra were

deconvoluted which showed bands around 300, 450, 685 and 770 cm^{-1} with varying intensities. Fig. 4b shows one of representative deconvoluted spectrum.

Spectra indicate the dominance of tellurium oxide glass network, which forms the backbone of this glass system. Doping with smaller amounts of RE^{3+} ions does not significantly shift the peak positions, but alters the intensity of bands indicating their role in creating non-bridging sites. It is well known that tellurium oxide rich glasses are made of different units of TeO$_4$ trigonal bipyramids (tbp), TeO$_{3+1}$ polyhedra, TeO$_3$ trigonal pyramids (tp) and Te-$_{eq}$O$_{ax}$-Te bonds. The ratios of these units get altered with the incorporation of different dopant atoms. In the present system of glasses, doping with holmium ions lead to the conversion of TeO$_4$ trigonal bipyramidal units into TeO$_3$ trigonal pyramidal units with an associated formation of non-bridging oxygen atoms [38,39].

Bands between 300 and 460 cm^{-1} correspond to bending modes of Te–O–Te, O–Te–O linkages in TeO$_4$ (tbps), owing to the combined effect of equatorial and axial oxygen atoms. The peaks observed around 686 and 771 cm^{-1} represent the stretching vibrational modes of trigonal bipyramidal and trigonal pyramidal/distorted TeO$_{3+1}$ units, respectively. Here the number $3 + 1$ indicates that the corresponding bond is longer than the three other bonds and is related to the formation of non-bridging atoms. Rare earth doping leads to change in the intensities of 771 cm^{-1} band and consequently alters the tellurium coordination from 4 to 3 by affecting the structure [40–43]. Holmium doping leads to the changes in intensity ratios of I$_{771}$/I$_{686}$ peaks indicating their role in modifying the structure between non-bridging and bridging atoms.

3.4. Absorption, luminescence analysis and hypersensitive transitions

The absorption spectra of holmium doped TZBB glasses in UV–Vis–NIR regions and the corresponding assignments originating from the ground level $^5I_8$ to various excited levels within the 4f shell are shown in Fig. 5. The absorption spectra contain ten transitions from $^5I_8$ → $^5I_7$, $^5I_6$, $^5F_5$, $^5S_2 + {}^5F_4$, $^5F_3$, $^5F_2$, $^5F_1 + {}^5G_6$, $^5G_5$, $^5G_4$ & $^4H_6$, with their corresponding wavelengths at 1949, 1172, 643, 539, 487, 471, 452, 419, 383 and 362 nm respectively. These are attributed to the 4f-4f

Table 2
Thermal parameters of Ho^{3+} doped barium tellurite glasses.

S. No.	Sample code	T_g (± 2 °C)	T_c (± 2 °C)	T_p (± 2 °C)	$\Delta T = T_c - T_g$ (± 2 °C)	$\Delta T_p = T_p - T_c$	$S = (\Delta T^* \Delta T_p)/T_g$
1	TZBBHo0.25	342	464	547	122	83	29.60
2	TZBBHo0.5	335	456	508	121	52	18.78
3	TZBBHo0.75	350	473	493	123	20	7.02
4	TZBBHo1.0	348	470	498	122	28	9.81
5	TZBBHo1.5	343	461	500	118	39	13.41
5	TZBBHo2.0	347	469	494	122	25	8.78

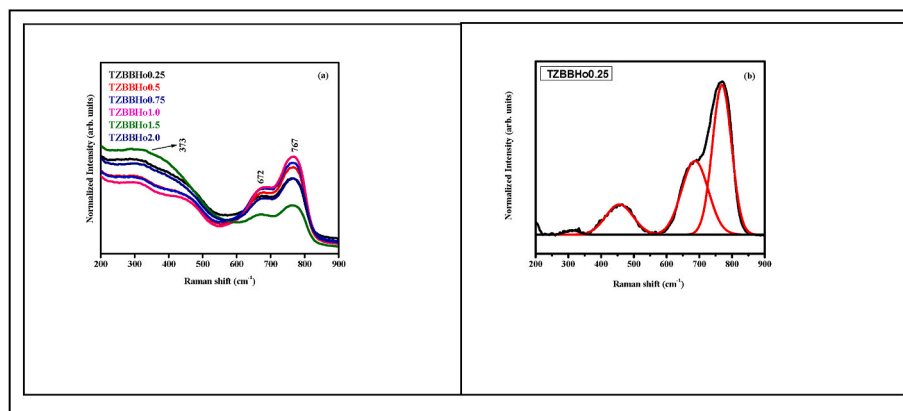**Fig. 4.** (a) Raman spectra of Ho^{3+} doped barium tellurite glasses & (b) Deconvoluted Raman spectrum of a representative sample.
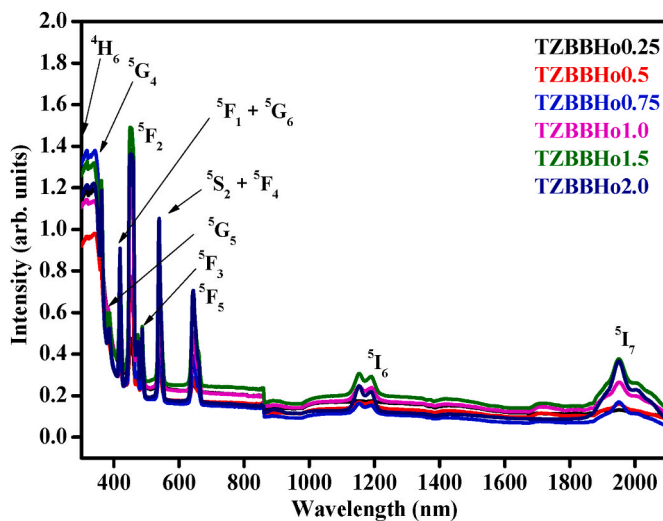
Fig. 5. UV–Vis–NIR absorption spectra of Ho^{3+} doped Barium tellurite glasses.

transitions of Ho^{3+} ions from the ground level to various excited levels. Incorporation of holmium ions leads to changes in intensity of these absorption bands, indicating the influence of doping in the glass matrix. Changes in the spectral characteristics of some absorption bands are also seen when the behaviour of neighbouring atoms of holmium differs. It is worth noting that the progressive intensification in holmium concentration in the glass series shields numerous distinctive absorption bands in the UV–Vis range [17,44,45].

Distinct visible and NIR transitions are shown below.

Visible region transitions

$^5I_8 \rightarrow {}^4H_6$, $^5I_8 \rightarrow {}^5G_4$, $^5I_8 \rightarrow {}^5G_5$, $^5I_8 \rightarrow 5F_1 + {}^5G_6$, $^5I_8 \rightarrow {}^5F_3$, $^5I_8 \rightarrow {}^5S_2 + {}^5F_4$, and $^5I_8 \rightarrow {}^5F_5$

NIR region transitions

$^5I_8 \rightarrow {}^5I_6$, and $^5I_8 \rightarrow {}^5I_7$

The identification and assignment of energy levels are made as per the procedure outlined by Carnall et al. [46]. The shielding effect of the 4f electrons of RE^{3+} ions is widely known and this shielding allows RE^{3+} ions to function as active centers in solid state laser hosts. These ions exhibit sharp absorption and luminescence transitions as surrounding ligand atoms weakly perturb them. The spectral intensities for the observed bands in these glasses, which are frequently described in terms of oscillator strength of forced electronic dipole transitions, were studied using Judd–Ofelt (JO) theory. The RE^{3+} ions have many absorption transitions from the ground state and are indicated in the UV–Vis–NIR

absorption spectra. These spectral data were utilized for calculating the experimental oscillator strength (f_{exp}) by considering the unified area under each absorption band with the help of the expression taken from literature [47–50]. The calculated oscillator strength values were utilized for calculating the J-O intensity parameters Ω_λ ($\lambda = 2, 4$ and 6) using least square fitting method. Furthermore, the calculated oscillator strength values were applied for the JO calculations and are presented in Tables 3 and 4. The accuracy between the calculated and experimental values of oscillator strength is defined by RMS value as shown in Table 3. J-O intensity parameters Ω_2, Ω_4 and Ω_6 were evaluated for all the prepared glass samples. The parameter Ω_2 is related to the covalence and coordination of the holmium ion (short-range effect), while Ω_4 and Ω_6 are determined by the effective Columbic interactions from the next coordination sphere. Ω_4 and Ω_6 values depend on bulk properties such as viscosity and dielectric value of the media and are also affected by the vibronic transitions of the RE^{3+} ions bound to the ligand atoms [15,51]. The values of Ω_4 and Ω_6 are strongly influenced by the vibrational levels associated with the central holmium ions bound to the ligand atoms. This results in the increase in the average Ho–O distance and produces a weaker field around holmium leading to decrease in the Ω_2 parameter for TZBB$_{2.0}$ ($\Omega_4 > \Omega_6 > \Omega_2$) sample. Majority of other samples, namely TZBB$_{0.25}$, TZBB$_{0.5}$, TZBB$_{0.75}$ & TZBB$_{1.5}$ follow the JO trend as $\Omega_2 > \Omega_4 > \Omega_6$, while TZBB$_{1.0}$ shows $\Omega_6 > \Omega_2 > \Omega_4$ [50–52]. Similar $\Omega_2 > \Omega_4 > \Omega_6$ trend has been observed in various holmium doped tellurite glasses, indicating the dominance of Ω_2 parameter [53–56]. Hypersensitive transition corresponding to $^5I_8 \rightarrow {}^5F_1 + {}^5G_6$, is observed from absorption spectra (Fig. 5) and are governed by the quadrupole selection rules ($\Delta S = 0$, ΔL, $\Delta J \leq 2$). The matrix element $\|U^2\|^2$ should be high for the hypersensitive transitions of electric dipole transitions. Non-uniform distribution around the RE^{3+} ion alongwith the magnitude of JO parameter Ω_2 can cause these hypersensitive transitions, whose values are higher [57].

Rare earth doped materials exhibit sharp excitation/emission bands. In this report, the luminescence spectra of all the holmium ion doped

Table 4
Calculated JO intensity parameter values $\Omega_\lambda(\lambda = 2,4,6)$ ($\times 10^{-20}$) of Ho^{3+} doped barium tellurite glasses.

S. No.	Sample Code	JO PARAMETERS			Trend of Ω_λ (λ = 2,4,6)
		Ω_2 ($\times 10^{-20}$) cm^2	Ω_4 ($\times 10^{-20}$) cm^2	Ω_6 ($\times 10^{-20}$) cm^2	
1.	**TZBBHo0.25**	1.57	1.30	1.14	$\Omega_2 > \Omega_4 > \Omega_6$
2.	**TZBBHo0.5**	5.22	2.72	1.85	$\Omega_2 > \Omega_4 > \Omega_6$
3.	**TZBBHo0.75**	7.52	4.73	1.85	$\Omega_2 > \Omega_4 > \Omega_6$
4.	**TZBBHo1.0**	1.98	1.09	3.17	$\Omega_6 > \Omega_2 > \Omega_4$
5.	**TZBBHo1.5**	3.94	3.43	1.97	$\Omega_2 > \Omega_4 > \Omega_6$
6.	**TZBBHo2.0**	2.86	3.33	1.63	$\Omega_4 > \Omega_6 > \Omega_2$

Table 3
Experimental and calculated oscillator strengths ($\times 10^{-6}$) of the Ho^{3+} doped barium tellurite glasses.

Wavelength (nm) and Transitions From $^5I_8 \rightarrow$	TZBBHo0.25		TZBBHo0.5		TZBBHo0.75		TZBBHo1.0		TZBBHo1.5		TZBBHo2.0	
	$f_{exp} \times 10^{-6}$	$f_{cal} \times 10^{-6}$	$f_{exp} \times 10^{-6}$	$f_{cal} \times 10^{-6}$	$f_{exp} \times 10^{-6}$	$f_{cal} \times 10^{-6}$	$f_{exp} \times 10^{-6}$	$f_{cal} \times 10^{-6}$	$f_{exp} \times 10^{-6}$	$f_{cal} \times 10^{-6}$	$f_{exp} \times 10^{-6}$	$f_{cal} \times 10^{-6}$
362 nm $\rightarrow {}^4H_6$	0.66	0.34	3.89	6.35	9.08	9.52	25.50	24.47	4.73	5.56	3.84	4.51
383 nm $\rightarrow {}^5G_4$	2.30	2.38	1.57	0.64	2.46	0.93	3.22	2.03	1.38	0.77	1.35	0.72
419 nm $\rightarrow {}^5G_5$	–	–	4.34	4.98	7.85	8.61	19.09	20.14	5.88	6.33	5.58	6.18
452 nm $\rightarrow {}^5F_1 + {}^5G_6$	11.64	11.67	33.71	33.45	49.76	49.76	127.19	127.27	29.48	29.45	23.89	23.87
471 nm $\rightarrow {}^5F_2$	0.63	1.51	2.29	2.66	3.35	2.99	3.47	5.89	3.29	2.82	3.32	2.36
487 nm $\rightarrow {}^5F_3$	2.60	1.19	1.68	1.92	2.50	1.92	5.17	3.30	2.35	2.07	2.40	1.72
539 nm $\rightarrow {}^5S_2 + {}^5F_4$	3.69	3.05	6.04	5.32	8.23	6.62	16.29	13.32	6.59	6.09	5.82	5.38
643 nm $\rightarrow {}^5F_5$	1.96	2.73	4.46	5.00	6.02	6.91	14.24	14.70	5.24	5.91	5.01	5.39
1172 nm $\rightarrow {}^5I_6$	0.75	1.06	1.47	1.77	0.99	1.89	2.36	3.48	1.47	1.92	0.93	1.62
1949 nm $\rightarrow {}^5I_7$	0.97	0.29	1.42	0.58	1.71	0.83	1.93	1.85	1.59	0.65	1.39	0.58
N	9		10		10		10		10		10	
σrms	0.70		0.96		0.93		1.52		0.58		0.64	

barium tellurite glasses were measured with 362 nm excitation wavelength and the prominent emission occurring between 350 and 700 nm is shown in Fig. 6. PL emission spectra of the prepared glasses recorded at this excitation wavelength yielded a strong green emission band along with weak red emission band for all concentrations. The first high intensity emission at 546 nm (green emission) corresponds to the $^5F_4$ ($^5S_2$)$\rightarrow^5I_8$, transition and the second considerable intensity peak at 659 nm (red emission) corresponds to the $^5F_5\rightarrow^5I_8$ transition. With increasing holmium concentration up to 0.75 mol%, the intensity of green emission increases, beyond which intensity decreases owing to concentration quenching effect. Such a condition has also been reported in different systems [13,14]. When the concentration of holmium increases, the ratio between number of bridging oxygen and non-bridging oxygen atoms changes which could be clearly seen in intensity ratio variations in Raman spectra. The resonant energy transfer and the non-resonant process between the levels $^5I_8$ & $^5F_4$ could be the prominent reason for explaining the concentration quenching behaviour at higher doping levels of holmium. Emission values indicate that the sample with 0.75 mol.% concentration is more suitable for lasing applications in the visible (green) region.

3.5. Radiative parameters and decay analysis

From the luminescence spectra, the emission transitions (SLJ $\rightarrow$ S'L'J'), energy gap (ΔE cm^{-1}), predicted radiative transition probabilities (A_R, s^{-1}), branching ratios (β_R), total radiative transition probabilities (A_T, s^{-1}) and the total decay times of various levels of TZBBHo glass series were evaluated and are presented in Tables 5 and 6. For choosing quality material aimed at laser applications the above-mentioned parameters are highly desired. The total radiative transition probability corresponding to green emission was found to be maximum for 1 mol.% of holmium doping, leading to least lifetime for $^5F_4$ ($^5S_2$) level. The predicted lifetime values were found to be different for each level with $^5I_7$ showing a larger lifetime for all concentrations, similar to various reported samples [44,45]. The lifetime values of prepared samples were evaluated from the graph of decay profiles measured for the excitation wavelength of 362 nm and are shown in Fig. 7a. The emission at 546 nm corresponding to the transition $^5F_4$ ($^5S_2$)$\rightarrow^5I_8$ is considered for the lifetime evaluation of Holmium doped TZBB samples. The decay profiles for all the prepared glasses analysed using the standard expression were found to be double exponential in nature [51,57]. It could be noticed that the lifetime decay value decreases for increasing holmium content with values of 17.68, 16.93, 14.83, 13.19, 10.60 and 10.05 ms for

corresponding samples of TZBBHo$_{0.25}$, TZBBHo$_{0.5}$, TZBBHo$_{0.75}$, TZBBHo$_{1.0}$, TZBBHo$_{1.5}$ and TZBBHo$_{2.0}$ respectively (Fig. 7b). Doping with holmium ions from 0.25 mol.% to 2 mol.% leads to a decrease in lifetime around 43%. Increasing the dopant concentration in the matrix causes more dipole-dipole interaction between the Ho-Ho neighbouring ions. This leads to increased possibility for energy transfer between them, which causes the transition $^5F_4$ ($^5S_2$)$\rightarrow^5I_8$ less radiative and hence a decrease in lifetime [44,52,53]. Measured lifetime of this glass system was found to be larger when compared with other glasses like fluorophosphates (5.87 ms) [17], lead phosphate (8.3 ms) [44], PbBiGa (4.79 ms) [58] etc. Also, the calculated quantum efficiency which is the ratio between the measured & calculated lifetimes was found to be above 60% for all concentrations, showing variations with holmium concentration. Higher value of lifetime and the quantum efficiency indicates the possibility of the present glass matrix as a suitable material for green laser applications.

Among all compositions, TZBBHo$_{1.0}$ sample showed the largest total transition probability and a smallest radiative decay time, though TZBBHo$_{0.75}$ exhibited the maximum emission intensity corresponding to green emission. Most of the reported results have been on samples with larger variations in rare earth ion concentrations or with standard 1 mol. % doping and hence showed consistent property changes at a particular composition [16,17,44]. However, observed variations in the physical and optical parameters between different samples in the present report can be correlated to closer variations in rare earth ion concentrations and are defined by the changes in bridging and non-bridging oxygen atoms around these compositions. The results indicate the need for compositional tuning depending on the application.

4. Nonlinear optical properties

4.1. Z-scan measurement: nonlinear absorption coefficient and optical limiting threshold

When high intensity light interacts with materials, optical nonlinearity develops resulting in nonlinear effects like self-focussing, self-defocussing, third harmonic generation etc. Third order nonlinear effects in these glassy samples were studied using Z-Scan setup proposed by Sheik-Bahae et al. [59,60]. The setup consists of a beam splitter, sample holder, focussing lens, detectors, translational stage and the laser source with a good Gaussian profile. A Q-switched frequency doubled Nd:YAG laser emitting 532 nm with a repetition rate of 10 Hz was used as the laser source. The beam splitter divides the laser beam into two, wherein one beam acts as a reference and the other falls on the sample focussed through a lens. The typical Z-Scan has two modes, namely open aperture and closed aperture. The open aperture can be used to study the nonlinear absorption, whereas the closed aperture yields both nonlinear absorption & nonlinear refraction, from which nonlinear refractive index (n_2) can be calculated. The absorption coefficient (β) is estimated via open aperture mode and experimental data is fitted to the theoretical curve using the equation proposed by Sheik-Bahae et al. [59,60]. Nonlinear absorption can be classified as either saturable or reverse saturable. Materials with a positive nonlinear absorption coefficient exhibit reverse saturable absorption (RSA), while those with negative nonlinear absorption coefficient exhibit saturable absorption (SA). RSA is characterized by high transmission at normal light intensities and a decrease in transmission under illumination of high intensity or high fluence. In general, RSA material is desirable for optical limiting application. Holmium doped barium tellurite glasses in open aperture configuration shows a deep valley indicating reverse saturable absorption nature which is required for optical limiting application (Fig. 8). Combined effect of two processes namely two photon absorption (2PA) and two step excited state absorption (ESA) can lead to this nonlinearity, wherein 2PA will be dependent on the laser excitation energy and the bandgap of the material. Considering that the bandgap of these materials lies close to energy of two photons, there is a possibility of
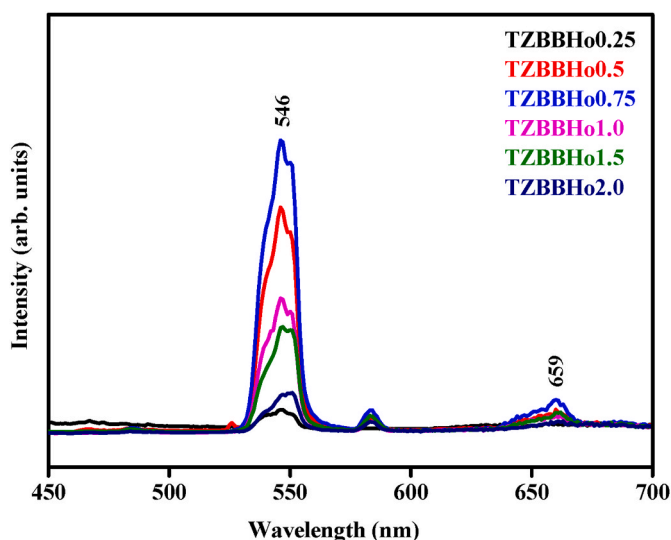

Fig. 6. Emission spectra of the Ho^{3+} doped barium tellurite glasses at 362 nm excitation wavelength.

Table 5
Emission transitions (SLJ → S'L'J'), energy gap (ΔE, cm^{-1}), predicted radiative transition probabilities (A_R, s^{-1}), and branching ratios (β_R) of various luminescent levels of TZBBHo glasses.

| TRANSITIONS | | ΔE | TZBBHo0.25 | | TZBBHo0.5 | | TZBBHo0.75 | | TZBBHo1.0 | | TZBBHo1.5 | | TZBBHo2.0 | |
S, L, J	S', L', J'		A_R	β_R	A_R	β_R	A_R	β_R	A_R	β_R	A_R	β_R	A_R	β_R
$^5S_2$	$^5F_5$	2861	0.86	0.002	1.67	0.0002	2.59	0.0004	1.19	0.0001	2.07	0.0003	1.97	0.0003
	$^5I_4$	5169	79.38	0.018	132.73	0.018	146.48	0.020	202.85	0.016	147.91	0.019	126.78	0.019
	$^5I_5$	7242	67.17	0.015	110.06	0.015	116.17	0.016	178.62	0.014	121.83	0.015	103.32	0.016
	$^5I_6$	9884	291.60	0.065	491.60	0.068	562.20	0.077	718.94	0.058	555.79	0.069	482.51	0.073
	$^5I_7$	13282	1748.71	0.388	2811.02	0.387	2796.65	0.382	4872.30	0.392	3065.76	0.386	2556.30	0.384
	$^5I_8$	18413	2314.59	0.514	3720.66	0.512	3701.64	0.505	6448.96	0.519	4057.84	0.510	3383.52	0.509
$^5F_5$	$^5I_4$	2308	0.17	–	0.27	–	0.37	–	0.23	–	0.31	–	0.30	–
	$^5I_5$	4381	15.37	0.004	25.89	0.003	29.91	0.003	35.03	0.004	28.32	0.003	24.56	0.003
	$^5I_6$	7023	187.21	0.045	323.87	0.043	388.13	0.037	429.70	0.054	364.32	0.040	319.16	0.039
	$^5I_7$	10421	764.65	0.184	1432.66	0.188	1981.10	0.190	1426.54	0.180	1677.13	0.186	1528.49	0.186
	$^5I_8$	15552	3190.24	0.767	5821.15	0.766	8007.90	0.769	6053.15	0.762	6943.82	0.770	6368.34	0.773
$^5I_4$	$^5I_5$	2073	15.90	0.084	22.93	0.075	25.22	0.080	30.13	0.060	24.64	0.073	22.05	0.078
	$^5I_6$	4715	72.20	0.379	118.18	0.386	123.08	0.390	194.22	0.384	129.90	0.387	109.54	0.387
	$^5I_7$	8113	84.35	0.443	136.54	0.446	138.85	0.440	231.18	0.458	149.72	0.446	125.63	0.443
	$^5I_8$	13244	17.85	0.938	28.70	0.094	28.56	0.091	49.73	0.098	31.30	0.093	26.10	0.092
$^5I_5$	$^5I_6$	2642	28.10	0.091	38.37	0.077	43.78	0.083	43.20	0.055	40.89	0.074	37.78	0.081
	$^5I_7$	6040	162.90	0.527	265.22	0.531	271.84	0.514	443.88	0.561	290.39	0.528	243.78	0.520
	$^5I_8$	11171	118.03	0.382	195.68	0.392	213.72	0.404	304.49	0.385	218.52	0.398	187.18	0.339
$^5I_6$	$^5I_7$	3398	59.51	0.158	81.54	0.134	88.87	0.137	103.78	0.110	87.14	0.132	79.14	0.140
	$^5I_8$	8529	316.34	0.842	525.81	0.866	558.50	0.863	837.60	0.890	575.71	0.869	486.14	0.860
$^5I_7$	$^5I_8$	5131	197.60	1.000	290.75	1.000	311.63	1.000	414.02	1.000	314.60	1.000	277.20	1.000

Table 6
Emission transitions (SLJ → S'L'J'), Total transition probability (ΣA_T), and radiative decay times ($\Sigma \tau_R$, μs) of various luminescent level of TZBBHo glasses.

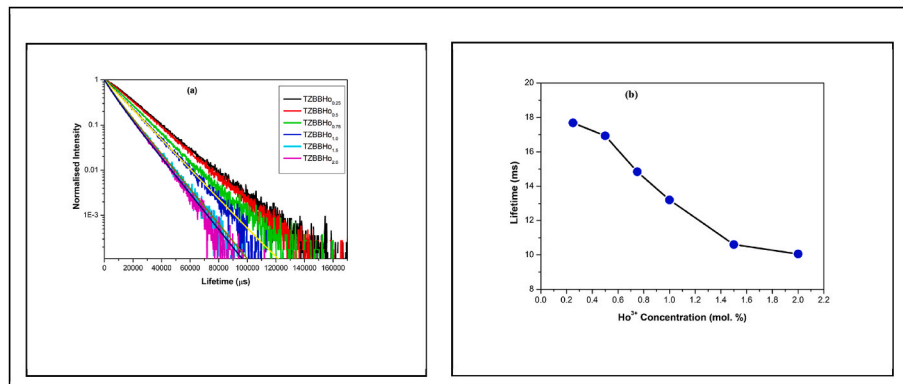| TRANSITIONS | | TZBBHo0.25 | | TZBBHo0.5 | | TZBBHo0.75 | | TZBBHo1.0 | | TZBBHo1.5 | | TZBBHo2.0 | |
S, L, J	S', L', J'	ΣA_T	$\Sigma \tau_R$	ΣA_T	$\Sigma \tau_R$	ΣA_T	$\Sigma \tau_R$	ΣA_T	$\Sigma \tau_R$	ΣA_T	$\Sigma \tau_R$	ΣA_T	$\Sigma \tau_R$
$^5S_2$	$^5F_5$	4502.30	222	7267.75	137	7325.74	136	12422.86	80	7951.19	125	6654.39	150
	$^5I_4$												
	$^5I_5$												
	$^5I_6$												
	$^5I_7$												
	$^5I_8$												
$^5F_5$	$^5I_4$	4157.64	240	7603.83	131	10407.42	96	7944.65	125	9013.90	110	8240.85	121
	$^5I_5$												
	$^5I_6$												
	$^5I_7$												
	$^5I_8$												
$^5I_4$	$^5I_5$	190.30	5254	306.36	3264	315.71	3167	505.25	1979	335.56	2980	283.32	3529
	$^5I_6$												
	$^5I_7$												
	$^5I_8$												
$^5I_5$	$^5I_6$	309.03	3235	499.27	2002	529.34	1889	791.57	1263	549.80	1818	468.74	2133
	$^5I_7$												
	$^5I_8$												
$^5I_6$	$^5I_7$	375.85	2660	607.34	1646	647.37	1544	941.38	1062	662.85	1508	565.28	1769
	$^5I_8$												
$^5I_7$	$^5I_8$	197.60	5060	290.75	3439	311.63	3208	414.02	2415	314.60	3178	277.20	3607

Fig. 7. (a) Luminescence decay curves & (b) concentration dependent lifetime variation of Ho^{3+} doped barium tellurite glasses.
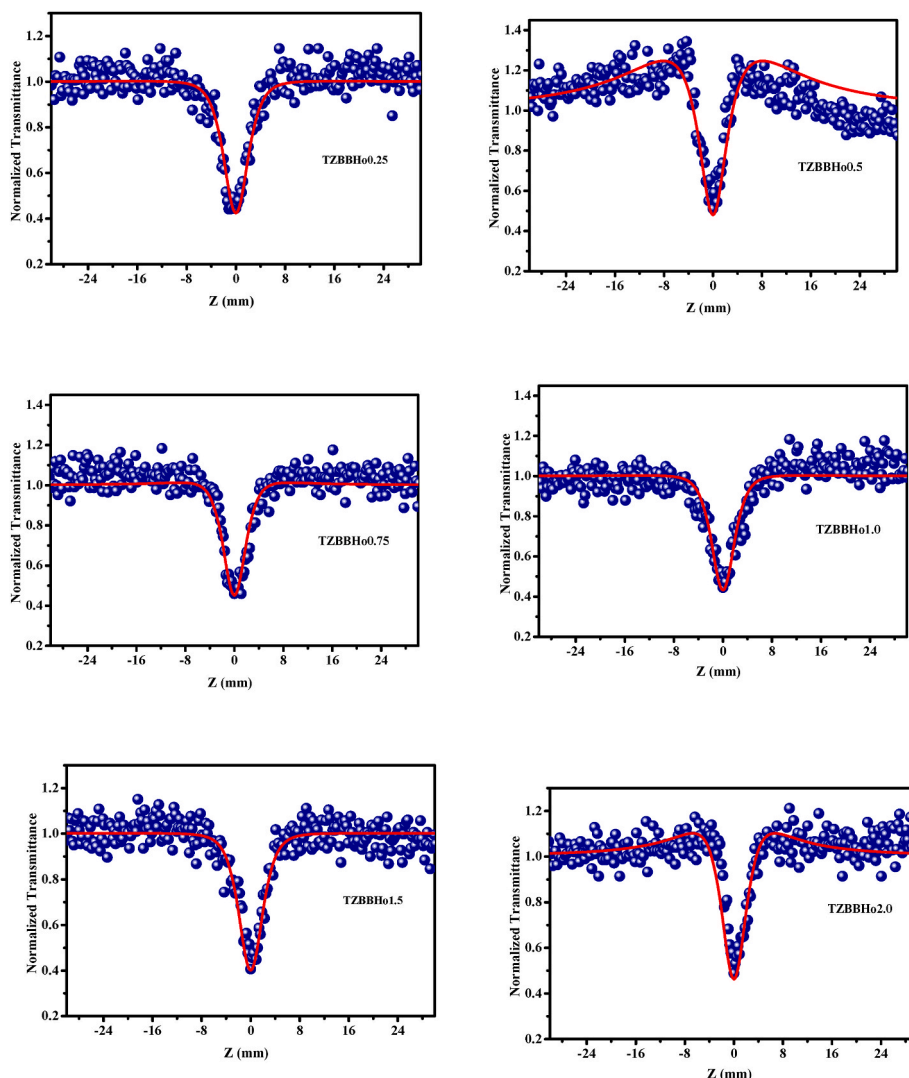
Fig. 8. Open aperture Z-Scan curves of Ho^{3+} doped barium tellurite glasses.

absorption of 2 photons in place of one photon leading to 2PA [22]. Presence of dopants also influences this process, as observed from β value variations between 0.870 and 1.090 with incorporation of holmium. The increase in nonlinear absorption coefficient can be attributed to changes in the ratio of non-bridging and bridging atoms in the network, the effect of which was visible in other studies also [22,23,61]. It has been stated that the valence electrons in non-bridging oxygen are less stable and are weakly bound to the host materials. Hence, the valence electrons are easily distorted by the laser's electromagnetic field which leads to an increase in nonlinear absorption coefficient. There is also a decrease in the nonlinear absorption coefficient for the concentrations 0.5 and 2.0 mol%, which can be attributed to the loss of a few photo carriers from the ground state. As a result, the nonlinear absorption coefficient decreases as the incident laser intensity exceeds saturation intensity [62].

The reduction in nonlinear absorption can be exploited for optical limiting application. Fig. 9 depicts the optical limiting curves, drawn as a function of input intensity (x-axis) vs output transmittance (y-axis). An important parameter to be calculated here is called limiting threshold. Lower the optical limiting threshold, the greater the efficiency of the optical limiting material. In nonlinear materials, laser light passes through them for lower input intensity but the materials become opaque for larger input intensity. This leads to potential application in the protection of eyes and detectors against excessive radiation as optical

limiters. The optical limiting experimental data is fitted for the corresponding equation to determine the limiting threshold of all the samples.

$$T(Z) = \frac{1}{\sqrt{\pi q(Z)}} \int_{-\infty}^{+\infty} ln\left[1 + q(Z)exp\left(-\tau^2\right)\right] d\tau$$

where $q(z) = \beta I_0 L_{eff}/[1+(z/z_0)^2]$ and β corresponds to the effective two-photon induced nonlinear absorption coefficient, I_0, the intensity of laser beam at the focal point, $L_{eff} = (1-exp(-\alpha_0 L))/(\alpha_0)$, the sample length, α_0 is linear absorption coefficient, $Z_0 = \frac{\pi \omega_0^2}{\lambda}$ is the Rayleigh range and ω_0 is the beam waist radius at Z = 0 [22]. The value of limiting threshold varies between 2.171 × 10^{12} W/m^2 to 4.701 × 10^{12} W/m^2. From Table 7, it can be concluded that the composition with 0.5 mol.% Holmium suits best for optical limiting applications among all concentrations. According to the current study, 2PA governs optical limiting in glass materials which has also been shown for various other glasses [21, 62,63]. Considering the properties exhibited by these holmium doped barium tellurite (TZBB) glasses, it could be emphasised that these glasses are highly suitable for optical limiting application, particularly in the nanosecond regime.
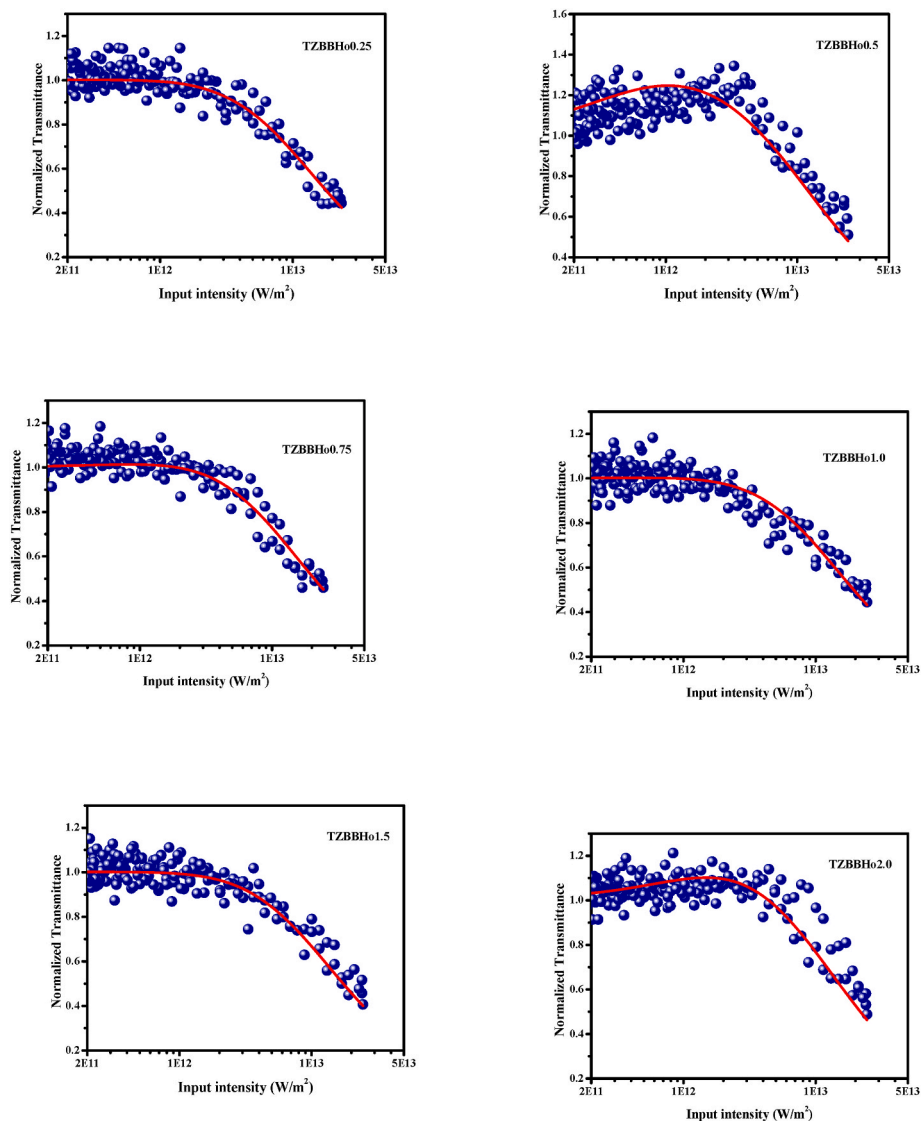
Fig. 9. Optical limiting curves of Ho^{3+} doped barium tellurite glasses.

Table 7

Two-photon absorption coefficient and Onset limiting threshold of Ho^{3+} doped barium tellurite glasses.

S. No.	Sample code	Non-linear absorption co-efficient β (× 10^{-10} m/W)	Limiting threshold (× 10^{12} W/m^2)
1.	**TZBBHo0.25**	0.99	3.325
2.	**TZBBHo0.5**	0.870	2.171
3.	**TZBBHo0.75**	0.920	4.701
4.	**TZBBHo1.0**	0.950	3.605
5.	**TZBBHo1.5**	1.090	3.402
6.	**TZBBHo2.0**	0.960	3.482

5. Conclusions

Barium tellurite glasses doped with holmium ions were investigated for their linear and non-linear optical properties. The possibility of applications as fiber optic devices was strengthened by their high thermal stability values. Refractive index values were found to be around 2.154 with the least value for 0.75 mol% of holmium, while the bandgap was found to be the largest for that composition. The changes around this composition indicated the transformation between non-bridging and bridging oxygen atoms owing to the influence of holmium ions. The intensity ratio variations in Raman spectra between the bands corresponding to bridging and non-bridging oxygen atoms also indicated the effect of dopant atoms. Green emission was found to be dominant among all measured transitions with the largest intensity at 0.75 mol%. The observed higher value indicates that this concentration is more suitable for lasing applications. Increasing dopant concentration leads to a decrease in lifetime of the energy levels. Presence of two photon absorption leads to reverse saturable absorption behaviour in these samples, which makes them suitable for optical limiting applications. Since different concentrations show the preferred values in lasing and limiting properties, compositional tunability is required to effectively utilize this tie-line of glasses for both lasing and non-linear optical applications.

CRediT authorship contribution statement

P. Vani: Investigation, Methodology, Formal analysis, Data curation, Writing – original draft. **G. Vinitha:** Methodology, Formal analysis, Writing – review & editing, Supervision. **R. Praveena:** Software, Data curation, Writing – review & editing. **M. Durairaj:** Investigation, Data curation. **T.C. Sabari Girisun:** Formal analysis, Writing – review & editing. **N. Manikandan:** Conceptualization, Methodology, Formal analysis, Data curation, Writing – review & editing, Supervision, Project administration.

Declaration of competing interest

Data availability

Data will be made available on request.

Acknowledgments

References

[1] Mohd. Azam, Deepak Kumar Mohanty, Vineet Kumar Rai, K. Singh, "Luminescence and Judd-Ofelt study of Ho^{3+}/Ho^{3+}-Yb^{3+} doped/codoped lead tellurite glasses for multifunctional applications, J. Lumin. 239 (2021), 118319.

[2] P. Rekha Rani, M. Venkateswarlu, K. Swapna, Sk. Mahamuda, M.V.V.K. Srinivas Prasad, A.S. Rao, Spectroscopic and Luminescence properties of Ho^{3+} ions doped Barium Lead Alumino Fluoro Borate glasses for green laser applications, Solid State Sci. 102 (2020), 106175.

[3] M. RaviPrakash, G. Neelima, Venkata Krishnaiah Kummara, N. Ravi, C.S. Dwaraka Viswanath, Subba Rao, S. Mahaboob Jilani, Holmium doped bismuth-germanate glasses for green lighting applications: a spectroscopic study, Opt. Mater. 94 (2019) 436.

[4] R. Cao, Y. Lu, Y. Tian, F. Huang, S. Xu, J. Zhang, Spectroscopy of thulium and holmium co-doped silicate glasses, Opt. Mater. Express 6 (2016) 2252.

[5] J.F. Sousa, R.T. Alves, F.G. Rego-Filho, A.S. Gouveia-Neto, Erbium to dysprosium energy transfer mechanism and visible luminescence in lead cadmium fluorogermanate glass excited at 405 nm, Chem. Phys. Lett. 723 (2019) 28.

[6] Akshatah Wagh, Vinod Hegde, G. Lakshminarayana, C.S. Dwaraka Viswanath, Y. Raviprakash, Sudha D. Kamath, The effects of γ-rays and electron beam on Eu^{2+} + Sm^{3+} and Eu^{3+} + Nd^{3+} co-doped lead fluoroborate glasses, Mater. Res. Express 5 (2018), 095204.

[7] J. Pisarska, M. Kuwik, A. Baranowska, M. Kochanowicz, J. Zmojda, P. Miliski, J. Dorosz, M. Lasniak, B. Starzyk, D. Dorosz, W.A. Pisarski, White light emission and energy transfer in Pr^{3+}/Er^{3+} co-doped InF$_3$ based glass, Mater. Res. Bull. 150 (2022), 111791.

[8] V. Tomar, R. Pandey, R. Singh, Influence of quenching rate and quenching media on formation of TeO_2 glasses, J. Mater. Sci. Mater. Electron. 32 (2021), 17726.

[9] P. Vani, G. Vinitha, M.I. Sayyed, B.O. Elbashir, N. Manikandan, Investigation on structural, optical, thermal and gamma photon shielding properties of zinc and barium doped fluorotellurite glasses, J. Non-Cryst. Sol. 511 (2019) 194.

[10] A. Kaur, A. Khanna, M. Gonzalez-Barriuso, Fernando Gonzalez, Thermal and light emission properties of rare earth (Eu^{3+}, Dy^{3+} and Er^{3+}), alkali (Li^+, Na^+ and K^+) and Al^{3+} doped barium tellurite and boro-tellurite glasses, J. Mater. Sci. Mater. Electron. 32 (2021), 17266.

[11] X. Wang, H. Li, L. Hu, Influence of Y_2O_3/Al_2O_3 ratio on structure and enhance emission properties of Ho^{3+} doped sol-gel high silica glasses, J. Lumin. 220 (2020), 117020.

[12] P.R. Rani, M. Venkateswarlu, K. Swapna, S. Mahamuda, M.S. Prasad, A.S. Rao, Spectroscopic and luminescence properties of Ho^{3+} ions doped Barium Lead Alumino Fluoro Borate glasses for green laser applications, Solid State Sci. 102 (2020), 106175.

[13] A. Pandey, H.C. Swart, Luminescence investigation of visible light emitting Ho^{3+} doped tellurite glass, J. Lumin. 169 (2016) 93.

[14] K. Mariselvam, J. Liu, Green emission and laser properties of Ho^{3+} doped titano lead borate glasses for colour display applications, J. Solid State Chem. 293 (2021), 121793.

[15] B. Suresh, Ya. Zhydachevskii, M.G. Brik, A. Suchocki, M. Srinivasa Reddy. M. Piasecki, N. Veeriah, Amplification of green emission of Ho^{3+} ions in lead silicate glasses by sensitizing with Bi^{3+} ions, J. Alloys. Cpds. 683 (2016) 114.

[16] C.R. Kesavalu, H.K. Kim, S.W. Lee, J. Kaewkhao, N. Wantana, S. Kothari, S. Kaewjaeng, Optical spectroscopy and emission properties of Ho^{3+} doped gadolinium calcium silicoborate glasses for visible luminescent device applications, J. Non-Cryst. Sol. 474 (2017) 50.

[17] V. Reddy Prasad, S. Damodaraiah, Y.C. Ratnakaram, Optical spectroscopy and luminescence properties of Ho^{3+} doped zinc fluorophosphate glasses for green luminescent device applications, Opt. Mater. 78 (2018) 63.

[18] J.J. Real, E. Rodriguez, C.G. Nava-Dino, M.C. Maldonado-Orozco, F. Gaxiola, R. Narro-Garcia, Effect of Ho^{3+} concentration on the luminescent and thermal stability of tellurite glasses, Mater. Res. Bull. 144 (2021), 111483.

[19] R.I. Miedzinski, Fuks-Janczarek, Y. El Sayed Said, Nonlinear optical properties of TeO_2-P_2O_5-ZnO-$LiNbO_3$ glass doped with Er^{3+} ions, Opt. Mater. 60 (2016) 456.

[20] L. Moreira, R.F. Falci, H. Darabian, V. Anjos, M.J.V. Bell, L.R.P. Kasab, C.D. S. Bordon, J.L. Doualan, P. Camy, R. Moncorge, The effect of excitation intensity variation and silver nanoparticle codoping on nonlinear optical properties of mixed tellurite and zinc oxide glass doped with Nd_2O_3 studied through ultrafast z-scan spectroscopy, Opt. Mater. 79 (2018) 397.

[21] P. Vani, G. Vinitha, N. Manikandan, Effect of dopants on the nonlinear optical properties of fluorotellurite glasses for optical limiting application, Phys. Scripta 96 (2021), 125804.

[22] P. Vani, G. Vinitha, K.A. Naseer, K. Marimuthu, M. Durairaj, T.C. Sabari Girisun, N. Manikandan, Thulium-doped barium tellurite glasses: structural, thermal, linear, and non-linear optical investigations, J. Mater. Sci. Mater. Electron. 32 (2021), 23030.

[23] M.S. Sajna, S. Perumbilavil, V.P. Prakashan, M.S. Sanu, C. Joseph, P.R. Biju, N. V. Unnikrishnan, Enhanced resonant nonlinear absorption and optical limiting in Er^{3+} ions doped multicomponent tellurite glasses, Mater. Res. Bull. 104 (2018) 227.

[24] N. Fatima, A.G. Pramod, P. Ramesh, K.N. Krishnakanth, G. Jagannath, S. Venugopal Rao, Y.F. Nadaf, Efficacy of Eu^{3+} on improving the near-infrared optical nonlinearities and optical limiting properties of antimony sodium borate glasses, J. Non-Cryst. Sol. 556 (2021), 120566.

[25] A. Pandey, V. Kumar, R.E. Kroon, H.C. Swart, Photon upconversion in Ho^{3+}-Yb^{3+} embedded tungsten tellurite glass, J. Lumin. 192 (2017) 757.

[26] R. El-Mallawany, I.Z. Hager, H. Mahfouz, H.A. Othman, Physical and mechanical investigations for bismuth tungsten tellurite glasses, J. Alloys Cpds. 883 (2021), 160802.

[27] A. Marzuki, R.A. Zikri, M.N.R. Jauhariyah, D.E. Fausta, Effect of Na_2O/PbO substitution on physical and optical properties of Er^{3+}-doped tellurite glasses, J. Phys. 19112 (2021), 012038.

[28] K.S. Shaaban, M.S.I. Koubisy, H.Y. Zahran, I.S. Yahia, Spectroscopic properties, electronic Polarizability, and optical basicity of titanium–cadmium Tellurite glasses doped with different amounts of lanthanum, J. Inorg. Organomet. Polym. Mater. 30 (2020) 4999.

[29] C.R. Kesavulu, H.J. Kim, S.W. Lee, J. Kaewkhao, N. Wantana, S. Kothan, S. Kaewjaeng, Optical spectroscopy and emission properties of Ho^{3+}-doped gadolinium calcium silicoborate glasses for visible luminescent device applications, J. Non-Cryst. Sol. 474 (2017) 50.

[30] S.A. Umar, M.K. Halimah, K.T. Chan, A.A. Latif, Physical, structural and optical properties of erbium doped rice husk silicate borotellurite (Er-doped RHSBT) glasses, J. Non-Cryst. Sol. 472 (2017) 31.

[31] A. Usman, M.K. Halimah, A.A. Latif, F.D. Muhammad, A.I. Abubakar, Influence of Ho^{3+} ions on structural and optical properties of zinc borotellurite glass system, J. Non-Cryst. Sol. 483 (2018) 18.

[32] E.A. Davis, N. Mott, Conduction in non-crystalline systems V. Conductivity, optical absorption and photoconductivity in amorphous semiconductors, Phil. Mag. 22 (1970), 0903.

[33] Y.C.R. Babu, P.S. Ramnaik, A.S. Kumar, Photoluminescence features of Ho^{3+} ion doped PbO-Bi_2O_3 borophosphate glass systems, J. Lumin. 143 (2013) 510.

[34] J. He, Z. Zhou, H. Zhan, A. Zhang, A. Lin, 2.85 µm fluorescence of Ho-doped water-free fluorotellurite glasses, J. Lumin. 145 (2014) 507.

[35] N. Manikandan, A. Ryasnyanskiy, J. Toulouse, Thermal and optical properties of TeO_2–ZnO–BaO glasses, J. Non-Cryst. Sol. 358 (2012) 947.

[36] K. Aishwarya, G. Vinitha, G.S. Varma, S. Asokan, N. Manikandan, Synthesis and characterization of barium fluoride substituted zinc tellurite glasses, Physica B: Cond. Mat. 526 (2017) 84.

[37] F. Wang, M. Cai, R. Chen, X. Jing, B. Li, Y. Tian, J. Zhang, S. Xu, The influence of TeO_2 on thermal stability and 1.53 µm spectroscopic properties in Er^{3+} doped oxyfluoride glasses, Spectrochim. Acta Part A: Mol. Biomol. Spec. 150 (2015) 162.

[38] G. Lakshminarayana, K.M. Kaky, S.O. Baki, A. Lira, P. Nayar, I.V. Kityk, M. A. Mahdi, Physical, structural, thermal, and optical spectroscopy studies of TeO_2-B_2O_3-MoO_3-ZnO-R_2O (R= Li, Na, and K)/MO (M= Mg, Ca, and Pb) glasses, J. Alloys Cpds 690 (2017) 799.

[39] G.S. Murugan, T. Suzuki, Y. Ohishi, Raman characteristics and nonlinear optical properties of tellurite and phosphotellurite glasses containing heavy metal oxides with ultrabroad Raman bands, J. Appl. Phys. 100 (2006), 023107.

[40] E.A. Lalla, M. Aznar, M. Konstantinidis, M.G. Daly, U.R. Rodríguez-Mendoza, Polarized Raman analyzes of (RE^{3+}) doped fluorotellurite glass and ceramics, Vib. Spectrosc. 103 (2019), 102934.

[41] E.A. Lalla, A. Sanz-Arranz, M. Konstantinidis, J. Freemantle, P. Such, A.D. Lozano-Gorrín, V. Lavin, G. Lopez-Reyes, F. Rull-Pérez, U.R. Rodríguez-Mendoza, Raman-IR spectroscopic structural analysis of rare-earth (RE^{3+}) doped fluorotellurite glasses at different laser wavelengths, Vib. Spec 106 (2020), 103020.

[42] S.N. Nazrin, M.K. Halimah, F.D. Muhammad, A.A. Latif, A.S. Asyikin, Impact of erbium-doped zinc tellurite glasses on Raman spectroscopy, elastic and optical properties, Chal. Lett. 18 (2021) 11.

[43] R.T. Alves, C.M. Trindade, N.O. Dantas, A.S. Gouveia-Neto, A.C.A. Silva, Structural disorder analysis via Raman spectroscopy in Ho3+/Pr3+ doped zinc tellurite glasses, J. Lumin. 241 (2022), 118522.

[44] Ch. Srininvasa Rao, Upendra Kumar, P. Babu, C.K. Jayasankar, Optical properties of Ho^{3+} ions in lead phosphate glasses, Opt. Mater. 35 (2012) 102.

[45] E. Rukmini, C.K. Jayasankar, Spectroscopic properties of Ho3+ ions in zinc borosulphate glasses and comparative energy level analyses of Ho3+ ions in various glasses, Opt. Mater. 4 (1995) 529.

[46] W.T. Carnall, P.R. Fields, K. Rajnak, Spectral intensities of trivalent lanthanide aquo ions", Pr^{3+}, Nd^{3+}, Pm^{3+}, Sm^{3+}, Dy^{3+}, Ho^{3+}, Er^{3+}, and Tm^{3+}", J. Chem. Phys. 49 (1968) 4424.

[47] M.J. Weber, Probabilities for radiative and nonradiative decay of Er^{3+} in LaF_{3}", Phys. Rev. 157 (1967) 262.

[48] M.P. Hehlen, M.G. Brik, K.W. Krämer, 50th anniversary of the Judd–Ofelt theory: an experimentalist's view of the formalism and its application, J. Lumin. 136 (2013) 221.

[49] G.S. Ofelt, Intensities of crystal spectra of rare-earth ions, J. Chem. Phys. 37 (1962) 511.

[50] B.R. Judd, Optical absorption intensities of rare-earth ions, Phys. Rev. 127 (1962) 750.

[51] M. Venkateswarlu, S. Mahamuda, K. Swapna, M.V.V.K.S. Prasad, A.S. Rao, S. Shakya, A.M. Babu, G.V. Prakash, Holmium doped Lead Tungsten Tellurite glasses for green luminescent applications, J. Lumin. 163 (2015) 64.

[52] E.A. Lalla, M. Konstantinidis, I. De Souza, M.G. Daly, I.R. Martín, V. Lavín, U. R. Rodríguez-Mendoza, Judd-Ofelt parameters of RE^{3+}-doped fluorotellurite glass (RE^{3+}= Pr^{3+}, Nd^{3+}, Sm^{3+}, Tb^{3+}, Dy^{3+}, Ho^{3+}, Er^{3+}, and Tm^{3+}), J. Alloys Cpds. 845 (2020), 156028.

[53] Marcin Sobczyk, Lukasz Matrek, Comparative study of optical properties of Ho^{3+} doped Re_2O_3-Na_2O-TeO_2 glasses, J. Lumin. 206 (2019) 308.

[54] Y. Zheng, B. Chen, J. Sun, L. Cheng, H. Zhong, X. Li, J. Zhang, Y. Tian, T. Yu, L. Huang, Composition dependent optical transitions and 2 μm emission properties of Ho^{3+} in $xGeO_2$-$(80-x)TeO_2$-$9.5ZnF_2$-$10BaF$-$0.5Ho_2O_3$ glasses, J. Rare Earths 29 (2011) 924.

[55] J.C. Boyer, F. Vegtrone, J.A. Capobianco, A. Speghini, M. Bettinelli, Optical transitions and upconversion properties of Ho^{3+} doped ZnO-TeO_2 glass, J. Appl. Phy. 93 (2003) 9460.

[56] B. Zhou, L. Tao, C.Y. Chan, W. Jin, Y.H. Tsang, E. Pun, Near and mid-infrared photoluminescence in Ho^{3+} doped and Ho^{3+} - Yb^{3+} codoped low phonon energy germane -tellurite glasses, J. Lumin. 137 (2013) 132.

[57] J. Yuan, T. Deng, P. Xiao, Y. Ye, W. Wang, Strong and broadband 2.7 μm fluorescence of Yb^{3+}/Er^{3+} codoped ZnO modified tungsten tellurite glasses for broadband mid-infrared optical amplifiers and tunable fiber lasers, J. Lumin. 246 (2022), 118840.

[58] X. Wang, L. Hu, W. Xu, S. Wang, L. Zhang, C. Yu, D. Chen, Spectroscopic properties of Ho^{3+} and Al^{3+} co-doped silica glass for 2 μm laser materials, J. Lumin. 166 (2015) 276.

[59] M. Sheik-Bahae, M.P. Hasselbeck, Third-order optical nonlinearities, Handbook of Optics" 4 (2000), 16-1.

[60] M. Sheik-Bahae, A.A. Said, T.H. Wei, D.J. Hagan, E.W. Van Stryland, Sensitive measurement of optical nonlinearities using a single beam, IEEE J. Quant. Electron. 26 (1990) 760.

[61] M.N. Azlan, M.K. Halimah, A.B. Suriani, Y. Azlina, R. El-Mallawany, Electronic polarizability and third-order nonlinearity of Nd^{3+} doped borotellurite glass for potential optical fiber, Mater. Chem. Phys. 236 (2019), 121812.

[62] M. Rao, V. Veeramohan, V. Ravi Kanth Kumar, N.K. Shihab, D. Narayana Rao, Third order nonlinear and optical limiting properties of alkaline bismuth borate glasses, Opt Laser. Technol. 107 (2018) 110.

[63] I. Fuks-Janczarek, R. Miedzinski, M. Reben, Linear and non-linear optical study of fluorotellurite glasses as function of selected alkaline earth metals doped with Er^{3+}", Opt Laser. Technol. 111 (2019) 184.